DOI: 10.1002/asia.200700020

Structure of the Michaelis Complex and Function of the Catalytic Center in the Reductive Half-Reaction of Computational and Synthetic Models of Sulfite Oxidase

Kuntal Pal, Pradeep K. Chaudhury, and Sabyasachi Sarkar*[a]

Abstract: By using frontier-molecular-orbital and electrostatic (nucleophilic) interactions as well as relaxed potential-energy surface scans, it is shown that the initial step in the oxygen-atom transfer (OAT) reaction of $[Mo^{VI}O_2(S_2C_2Me_2)SMe]^{-1}$ (**1**) and $[Mo^{VI}O_2\{(S_2C_2(CN)_2\}_2]^{2-}$ (**2**) with HSO_3^- takes place by oxoanionic binding of the substrate to the Mo^{VI} center with the formation of a stable Michaelis complex. The gas-phase and solvent-corrected enthalpy profile with fully optimized minima and transition states for the OAT reaction of **1** and **2** with HSO_3^- showed the release of reaction energy for both complexes. The optimized geometries of **1** and **2** in the respective enzyme–substrate complexes showed a common feature with the participation of hydrogen bonding of the substrate with the axial (spectator) oxo group in the subsequent formation of the six-membered MoO_2HOS transition state. The enzyme–substrate complex of **2** shows heptacoordination as proposed earlier, although the *trans* (to axial oxo)-Mo–S(dithiolene) bond is elongated to 2.948 Å.

Keywords: cofactors · computational models · density functional calculations · Michaelis complex · sulfite oxidase

Introduction

Mononuclear molybdoenzymes play an important role in biology by catalyzing oxygen-atom transfer (OAT) reactions to maintain mainly the global nitrogen, sulfur, and carbon cycles.[1,2] All these enzymes contain a molybdenum cofactor that comprises either one or two organic moieties of molybdopterin (MPT) or some of its nucleotide variants, each of which is coordinated to molybdenum with an enedithiolene motif. On the basis of the different number of enedithiolene groups coordinated to the central Mo atom, these enzymes are generally classified into three separate families as xanthine oxidase,[3] DMSO (dimethyl sulfoxide) reductase,[4] and sulfite oxidase.[5–12] In the sulfite oxidase (SO) family, hepatic sulfite oxidase is an extensively studied molybdoenzyme with direct relevance to human health.[5] SO deficiency may lead to neurological problems, mental retardation, and dislocation of the ocular lens.[6] The physiological role of SO is to detoxify sulfite by oxidizing it to sulfate through OAT in the terminal step of the oxidative degradation of S-containing amino acids. This reaction is coupled with mitochondrial oxidative phosphorylation; both processes share cytochrome c as the common gateway to shuffle the electrons generated by sulfite oxidation to the terminal electron acceptor, molecular oxygen, via cytochrome c oxidase. Native SO follows typical Michaelis kinetics[7] with anionic binding of the substrate (sulfite) to form the enzyme–substrate complex according to the reductive half-reaction [Eq. (1)]:

$$E + S \rightleftharpoons [ES]^{\pm} \rightleftharpoons [ES] \rightleftharpoons [E'P]^{\pm} \rightleftharpoons [E'P] \rightleftharpoons E' + P \qquad (1)$$

in which E = enzyme, S = substrate, E′ = reduced enzyme, and P = product.

With sulfate ion as the product showing competitive inhibition and hydrogen phosphate ion present in mitochondria as inorganic phosphate showing mixed noncompetitive inhibition, the kinetic studies of such inhibitions can be explained by anionic binding of the substrate to the Mo center of the active site.[8] On the basis of several spectroscopic studies[9] followed by X-ray single-crystal structure determination with 1.8-Å resolution for the reduced state,[10] the nature of the Mo cofactor (Mo-co) present in SO has now been fully characterized. The reduced form of Mo-co under regeneration of the oxidized enzyme supposedly contains a

[a] K. Pal, Dr. P. K. Chaudhury, Prof. Dr. S. Sarkar
Department of Chemistry
Indian Institute of Technology, Kanpur
Kanpur 208016 (India)
Fax: (+91) 512-559-7265
E-mail: abya@iitk.ac.in

Supporting information for this article is available on the WWW under http://www.chemasianj.org or from the author.

cis-dioxo Mo^{VI} moiety with one oxo group at the axial position and another on the equatorial plane in a square-pyramidal geometry. The remaining three equatorial positions are occupied by three S atoms (bisdithiolene from molybdopterin[9b] and one from cysteine). This cysteine is a part of the protein chain, and MPT is a discrete organic moiety that comprises an enedithiolene functionality coordinated to the central molybdenum atom present in the active site and structurally placed there by several noncovalent H-bonding interactions with the protein. The cysteine and dithiolene moieties have been implicated in the tuning of the flexibility of the equatorial oxo group towards the OAT reaction.[11]

Several model complexes with the $(MoO_2)^{2+}$ group have been obtained by using different donor-atom environments.[12–14] Most of these complexes responded to the OAT reaction with phosphines as the "proxy" substrate, but almost all failed to react[13] with the native substrate, the sulfite (or hydrogen sulfite) ion. All these OAT reactions involving phosphine derivatives follow typical second-order kinetics[14] without the involvement of the Michaelis complex, with saturation kinetics prevalent in these enzymatic reactions.

Enough considerations were made to understand the nature of the mechanistic path involved in the OAT reaction. As phosphines were found to be good oxo acceptors from molybdenum-bound oxo groups, the reaction of complexes such as $[MoO_2(XY)_2]^{n-}$ (donor atom; X = N, S; Y = S, S) with PR_3 were studied in detail. It was proposed[14a] that the attack of the lone-pair electrons of PR_3 on the Mo=O group present in the $Mo^{VI}O_2$ moiety in such complexes leads to the OAT reaction through an associative pathway. Such complexes were also studied in the initial computational analysis of the OAT of $Mo^{VI}O_2$ centers by Pietsch and Hall,[15a] which were subsequently extended.[15b–d] Recently, isolation of an intermediate complex with an Mo^{IV}–O_{eq}–PEt_3 bond supported such a mechanism.[16] But proper inspection of the Mo–O_{eq} and O_{eq}–P bond lengths as 2.157 and 1.516 Å in this complex, respectively, revealed that, by definition, it is not an ES complex; rather it is a complex analogous to E′P [Eq. (1)]. Hence, any mechanism that does not involve the formation of a Michaelis complex cannot explain an enzymatic reaction with Michaelis–Menten kinetics.

Abstract in Bengali:

অ্যাবস্ট্র্যাক্টঃ ফ্রন্টিয়ার মলিকিউলার অর্বিটাল (FMO), ইলেক্ট্রোস্ট্যাটিক (নিউক্লিয়ফিলিক) ইন্টার‍্যাকশন এবং রিল্যাক্সড পোটেনটিয়াল এনার্জি সারফেস (PES) স্ক্যান দ্বারা দেখানো হয়েছে যে HSO_3^- এর সাথে $[Mo^{VI}O_2(S_2C_2Me_2)SMe]^{1-}$ (**1**) অথবা $[Mo^{VI}O_2\{(S_2C_2(CN)_2\}_2]^{2-}$ (**2**) এর অক্সিজেন অ্যাটম ট্রান্সফার রিয়্যাকশনের (OAT) প্রাথমিক ধাপ সাবস্ট্রেটের সাথে Mo(VI) সেন্টারের অক্সো-অ্যানায়নিক বন্ধন দ্বারা স্থিতিশীল "মিকাইলিস কমপ্লেক্স" তৈরি হওয়ার মাধ্যমে সংঘটিত হয়। গ্যাসীয় অবস্থা এবং 1 ও 2 এর সাথে HSO_3^- এর OAT রিয়্যাকশনের ট্রানজিশন স্টেট ও সম্পূর্ণ ভাবে অপটিমাইজড মিনিমা সম্বলিত সলভেন্ট কারেক্টেড এনথ্যালপি প্রোফাইল থেকে যথাক্রমে **1** ও **2** এর রিয়্যাকশন এনার্জি মুক্ত হওয়া দেখা গেছে। **1** ও **2** এর ট্রানজিশন স্টেটের অপটিমাইজড জিওমেট্রি থেকে সাবস্ট্রেটের সাথে অ্যাক্সিয়াল (স্পেকটেটর) অক্সো গ্রুপের হাইড্রোজেন বন্ধনী এবং পরবর্তী ধাপ হিসাবে ছয় সদস্যের (MoO_2HOS) ট্রানজিশন স্টেট তৈরি হওয়ার মতো ঘটানার মিল দেখা গেছে। **2** সম্বলিত ট্রানজিশন স্টেটের ক্ষেত্রে পূর্বে প্রস্তাবিত সাত সদস্যের ট্রানজিশন স্টেট দেখা গেছে যদিও ট্রান্স (অ্যাক্সিয়াল অক্সো-এর সাপেক্ষে) Mo – S (ডাইথায়োলিন) বন্ধনীটি 2.948 Å অবধি বর্ধিত হয়েছে। এক ছোট, কম মলিকিউলার ওজনের ইনরগ্যানিক মডেল কমপ্লেক্স বিশাল মলিকিউলার ওজনের নেটিভ সালফাইট অক্সিডেজের মতই এনজাইমেটিক কাইনেটিক্স দেখায়। রিয়্যাকশন প্রোফাইল অনুসরণ এবং "মিকাইলিস কমপ্লেক্স"-এর গঠন প্রতিষ্ঠিত করার মাধ্যমে ডেনসিটি ফাংশনাল থিওরি লেভেলের ক্যালকুলেশন দ্বারা এইরকম মডেল রিয়্যাকশনের কাইনেটিক ম্যানিফেস্টেশন পরীক্ষিত হয়েছে।

Amongst all the model complexes, the unique complex $[Bu_4N]_2[Mo^{VI}O_2(mnt)_2]$ (**2**; mnt = maleonitriledithiolate) mimics the active-site function of SO by undergoing OAT with the physiological substrate HSO_3^- both in terms of saturation kinetics as well as the inhibition patterns with SO_4^{2-} and $H_2PO_4^-$ anions.[17] Interestingly, **2** on reaction with phosphine[14c,18] followed typical second-order kinetics similar to those of other model complexes. On the basis of the enzymatic reaction of **2** toward the native substrate, hydrogensulfite ion, a mechanism was proposed: the substrate oxoanion binds to Mo^{VI}, which leads to the formation of a heptacoordinated Michaelis-type complex and, subsequently, product formation with the dissociation of the reduced form of **2**.

With native SO, an alternative neutral substrate, dimethyl sulfite, was used at pH > 7, which implicates attack of the lone-pair electrons as the critical step.[19] To accommodate the formation of a Michaelis complex, interaction between the approaching substrate with the amino acid residues present near the active sites was invoked. Such interpretation certainly underscores, at least in the case of the native enzyme, the importance of substrate oxoanionic binding to the Mo^{VI} center as being an essential criterion for the observation of Michaelis–Menten kinetics.

On the basis of phosphine-oxidation reactions, density functional theory (DFT) computational studies were initiated. Nordlander and co-workers proposed[20] that this OAT reaction takes place through attack of the sulfur lone-pair electrons (of hydrogensulfite) on one of the oxo groups of **2**. However, the possibility of oxoanionic attack on the Mo center was not taken into consideration in this study. This proposed reaction mechanism led Kirk and co-workers to suggest[21] the attack of the S lone-pair electrons (of sulfite) on the Mo=O_{eq} antibonding orbital, which is analogous to phosphine oxidation, by using the computational model complex $[Mo^{VI}O_2(S_2C_2Me_2)(SMe)]^-$ (**1**).

To mimic the chemistry of native SO, that is, the attack of the sulfur lone-pair electrons of the neutral molecule, the reaction of dimethylsulfite with **2** was tested at pH 7, but no OAT reaction occurred.[22] This was possibly due to the poor basicity of the sulfur lone-pair electrons of dimethylsulfite relative to the phosphorus lone-pair electrons of PPh_3. However, it was shown that $(CH_3O)_2SO$, at a pH identical to that used in the kinetic study of native SO with $(CH_3O)_2SO$ (pH $\approx$ 8),[19] responded with similar kinetics, and the real substrate was found to be the hydrolyzed product, sulfite ion formed from $(CH_3O)_2SO$. This hydrolysis may be responsible for the alleged reactivity of $(CH_3O)_2SO$ with native SO, for which the kinetic constants match very well with those found for sulfite ion as the substrate with native SO[8].

The mechanism of the OAT reaction involving sulfite oxidation has, therefore, not yet been clearly understood. Two important points are still to be determined. The first is if the initial attack of the substrate, HSO_3^-, is oxoanionic or lone-pair-electronic in nature (Scheme 1).[23] The second is the mechanistic features involved in the electronic rearrangements within the ES complex to yield E′ and P [Eq. (1)]. The proper visualization of the ES complex turned out to be

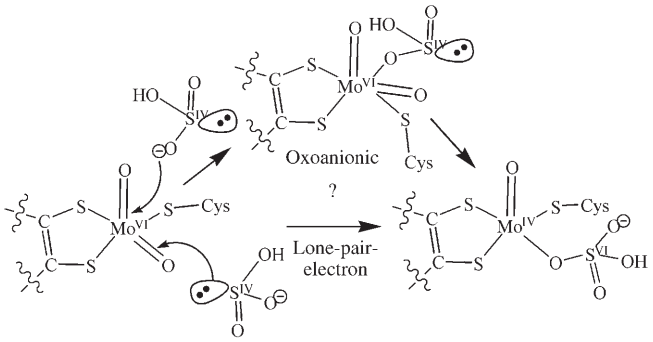

Scheme 1. Two possible forms of initial attack of HSO_3^- on Mo-co of sulfite oxidase.

of potential interest. DFT investigations into the nature of the ES complex in the catalytic cycles of DMSO reductase, trimethyl *N*-oxide reductase, and nitrate reductase have been reported.[24] In this paper, we investigate the nature of the ES complex in the catalytic cycle of SO.

Herein we report a theoretical study based on DFT calculations to investigate the plausibility of the formation of a Michaelis (ES) complex by "reaction" of the substrate HSO_3^- with the computational model complex **1** ($[Mo^{VI}O_2(mpt)Cys]^{-1}$) of Mo-co, derived from the X-ray structure of SO, and with the experimental model complex **2** through oxoanionic attack of HSO_3^-. We subsequently computed the gas-phase- and solvent-corrected enthalpy profiles for the half-reaction of HSO_3^- oxidation by **1** and **2**.

Results and Discussion

The earliest kinetic investigation into the reaction of native SO with sulfite showed that this reaction displayed Michaelis kinetics with sulfate as competitive (product inhibitor) and monohydrogenphosphate ion as mixed competitive inhibitors.[9] The model complex **2** was shown to follow a very similar kinetic pattern on reaction with HSO_3^- followed by very similar inhibitions with sulfate and monohydrogenphosphate ion.[17] Unlike SO, **2** does not have any protein component, and its response with similar kinetics strongly supports the proposition that with native SO, Mo-co is sufficient for binding the substrate without much intervention of the amino acids present near the active site. On this basis, the direct interaction between substrate and enzyme is taken into consideration for the formation of the intermediate ES complex. The electronic properties of the substrate and the enzyme (Mo-co) play an important role in the description of this interaction. It is clear that the nature of the lowest unoccupied molecular orbital (LUMO), which is the potential electron acceptor of the enzyme, and the highest occupied molecular orbital (HOMO) of the substrate are the focus.

The DFT (B3LYP)-optimized geometry of Mo-co was found to be square pyrimidal with an Mo–O_{eq} bond length of 1.720 Å, an average Mo–S(dithiolene) bond length of 2.519 Å, and an Mo–S(Cys) bond length of 2.457 Å. The Mo–O_{ax} bond (1.743 Å) is slightly longer (0.023 Å) than the Mo–O_{eq} bond. The cysteinyl group is oriented with a torsion angle (O_{ax}–Mo–S–C(Cys)) of 58°. However, in the X-ray structure of SO, the O_{ax}–Mo–S–C(Cys) torsion angle is 77°, which can be interpreted as due to the change in protein conformation during the crystallization process; this has been observed in the solid state. The Mo-co model structure used in this work structurally resembles the synthesized structural model complex of SO.[25]

Molecular-orbital analysis of the optimized geometry of Mo-co showed interesting results. The LUMO of Mo-co is predominately populated by the d_{xy} orbital of the central Mo atom (from the antibonding interaction between 60% d_{xy}(Mo), 11% p(O_{eq}), and 4% p(O_{ax}) orbitals; Table 1). The

Table 1. Calculated atomic-orbital coefficients for selected molecular orbitals.

LUMO of model complexes	Mo [%] (orbital)	O_{ax} [%] (orbital)	O_{eq} [%] (orbital)
Mo-co	60.48 (d_{xy})	3.45 (p)	11.23 (p)
1	55.23 (d_{xy})	8.63 (p)	15.44 (p)
2	43.08 (d_{xy})	11.06 (p)	10.99 (p)
HOMO of substrate	S [%] (orbital)	Oxoanion [%] (orbital)	O [%] (orbital)
HSO_3^-	40.12 (s)	23.3 (p)	19.89 (p)

HOMOs of HSO_3^- and PPh_3 are entirely different. The HOMO of HSO_3^- comprises 40% s(S), 23% p(O anionic), and 20% p(O) (the negative charge of HSO_3^- is distributed over two equivalent oxo groups). The HOMO of PPh_3 is predominantly viewed as the lone-pair orbital of the P atom. By considering frontier-molecular-orbital (FMO) interaction between the HOMO of HSO_3^- and the LUMO of Mo-co, two interactions, one between d_{xy}(Mo) of the LUMO and p(O) of the HOMO (Figure 1, interaction 1) and the other between p(O_{eq}) of the LUMO and S of the HOMO (Figure 1, interaction 2), are possible. However, similar FMO interaction is not possible with phosphine. The so-called phosphine lone pair of electrons can interact with the Mo=O_{eq} antibonding MO to facilitate the cleavage of the Mo–O_{eq} bond by a one-step process; this may lead to a different mechanism that may follow typical second-order kinetics.

From population analysis of partial-charge partitioning (Mulliken and natural bond orbital (NBO); Table 2), it was found that the interaction between the anionic oxo group of HSO_3^- and the Mo center of Mo-co is stronger than that between the S lone-pair electrons of HSO_3^- and the O_{eq} atom of Mo-co. This suggests that the Mo center is more susceptible to nucleophilic attack by the oxoanion of HSO_3^- than the O_{eq} atom of Mo-co is to lone-pair-electron attack of the S atom of HSO_3^-, because of a larger difference in formal charge that results in stronger electrostatic interaction. This interaction was taken into account in the light of the anionic charged substrate for SO.[20] The calculated Mulliken and NBO atomic charges are listed in Table 2. These results

CHEMISTRY
AN ASIAN JOURNAL

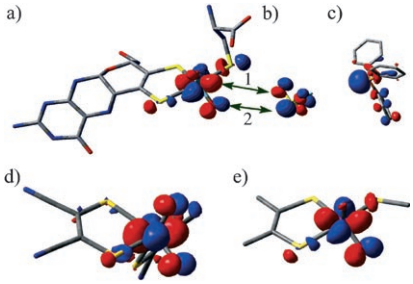

Figure 1. MO isosurface: a) LUMO of Mo-co; b) HOMO of HSO_3^-, arrows indicate the FMO interaction of the same phase, 1 corresponds to the interaction between the d_{xy}(Mo) orbital and the p(O) orbital of HSO_3^-, 2 corresponds to the interaction between O_{eq} and the S atom of HSO_3^-; c) HOMO of PPh_3 showing only one possible interaction; d) LUMO of **2**; e) LUMO of **1** showing close analogy with the LUMO of Mo-co. Hydrogen atoms are omitted for clarity.

Table 2. Calculated Mulliken and NBO atomic charges of enzyme model complexes and substrate.

	Mulliken charge			NBO charge		
Substrate	S	O	Oxoanion	S	O	Oxoanion
HSO_3^-	0.79	−0.75	−0.7	1.52	−1.01	−0.99
Model complexes	Mo	O_{ax}	O_{eq}	Mo	O_{ax}	O_{eq}
Mo-co	0.68	−0.49	−0.65	1.16	−0.60	−0.52
1	0.34	−0.47	−0.57	1.16	−0.47	−0.56
2	0.48	−0.49	−0.46	0.55	−0.49	−0.47

demonstrate that the FMO and electrostatic interactions could lead to a preference for oxoanionic attack in the formation of the ES complex. The relative stability of the ES complex and of other reaction intermediates and their transition states dictates the true reaction mechanism. Such detailed studies with Mo-co require much computational resources. To decrease the computational effort, we chose two model complexes: the computational model **1** and the unique functional model **2**. Full reaction pathways for the reactions of **1** and **2** with HSO_3^- were established.

The optimized geometry of **1** is very similar to that of the Mo-co model and matches the reported geometrical parameters.[21] Here the Mo–O_{ax} bond length also differs slightly from the Mo–O_{eq} bond length, but this difference is less (0.001 Å), as it is caused by the weak H-bonding interaction between the CH_3 and axial oxo groups. However, the orientation of the SCH_3 group differs with respect to the cysteinyl sulfur atom, as found from the X-ray structure analysis on native SO. We performed a relaxed 1D potential-energy surface (PES) scan of the dihedral angle O_{ax}–Mo–S–C_{Me} with a variation of 10° at each step at which all other parameters were allowed to optimize. A plot of the change in total energy versus the variation of the O_{ax}–Mo–S–C_{Me} dihedral angle is shown in Figure 2. It was found that three high-energy conformers exist at dihedral angles of 120°, 0°, and −120°, and two low-energy conformers exist at −60° and 60°; the lowest-energy structure has an O_{ax}–Mo–S–C_{Me} dihedral angle of −60°. In native SO, this dihedral angle was found to be 77° from the solid-state crystal structure data. Although the crystallization began with a solution of the oxidized enzyme, it was the reduced enzyme that finally crystallized out.[10] We are not certain of the preference in the orientation of cysteine present in the protein for the different redox states of the enzyme in solution. At this stage, we proceeded with our study on the basis of the fact that the model complex **2** responds to similar enzymatic reactions without the intervention of any protein. The molecular-orbital-feature and population analyses (Mulliken and NBO) of the atomic charge for **1** and **2** are very similar to that found for the Mo-co model. The LUMOs of **1** and **2** are shown in Figure 1. A list of the calculated atomic-orbital coefficients for selected molecular orbitals and the atomic charges are provided in Tables 1 and 2.

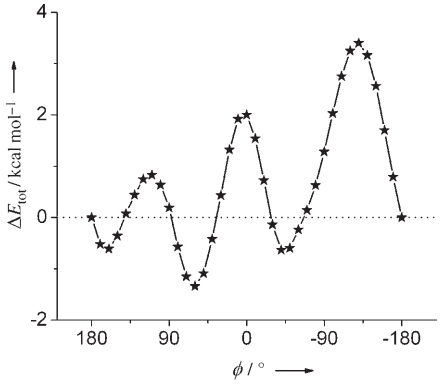

Figure 2. 1D relaxed PES scan of O_{ax}–Mo–S–C_{Me} dihedral angles (ϕ) for **1**.

The nature of oxoanionic and lone-pair-electron attack of HSO_3^- were checked by performing relaxed 1D PES scans for **1** and **2** (Figure 3). For oxoanionic attack, the anionic oxygen atom of HSO_3^- was placed 3.5 Å from the Mo center, and this distance was decreased in several fixed steps with geometry optimization at each step while the remaining degrees of freedom were allowed to vary. For lone-pair-electron attack, the S atom of HSO_3^- was placed 3.5 Å from the O_{eq} group of sulfite, and the same treatment was carried out as for anionic attack. In this case (Figure 3b), the reaction proceeded through one potential-energy barrier and finally reached a lower energy state in which the Mo–O_{eq} and O_{eq}–$S_{sulfite}$ bond lengths were 2.4 and 1.5 Å, respectively, which suggests completion of the OAT reaction. The lone-pair-electron attack is thus a one-step process similar to phosphine oxidation and so cannot be the enzymatic reaction. In contrast, for oxoanionic attack at the Mo center (Figure 3a), the relaxed PES scan results showed a relatively stable intermediate at an equilibrium Mo–$O_{sulfite}$ bond length of 2.2 Å. There was no further change in the Mo–O_{eq} bond length throughout the scan. At this stage, there is no lengthening of the Mo=O_{eq} bond and the S atom is directed toward the O_{eq} group, and this energy-minimized state can be considered as an ES complex before OAT. A second scan was performed on the energy-minimized state of the first scan with

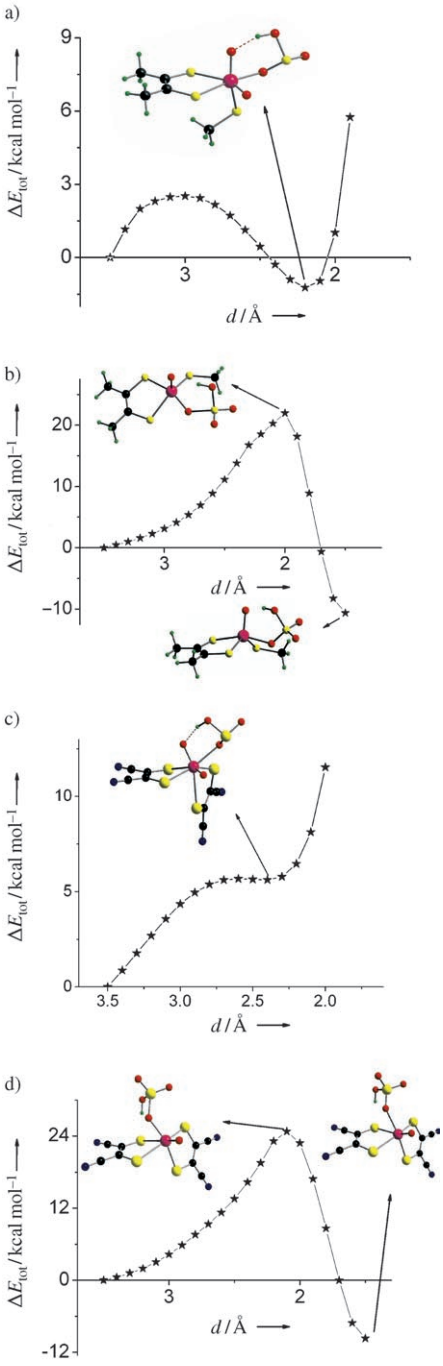

Figure 3. 1D relaxed PES scan (plot of total energy vs. scanning bond length): a) oxoanionic attack of HSO_3^- on **1**; b) lone-pair-electron attack of HSO_3^- on **1**; c) oxoanionic attack of HSO_3^- on **2**; d) lone-pair-electron attack of HSO_3^- on **2**. The changes in selected bond lengths for the scan are given in the Supporting Information.

decreasing S–O_{eq} bond length, and this process went past a second energy barrier to form the product. Similar results were found for the functional analogue complex **2** (Figure 3c and d). The changes in selected bond lengths for each scan are listed in the Supporting Information. Thus, from FMO interactions and from the relaxed PES scan, it is concluded that the initial step of the OAT reaction with **1** or **2** takes place by oxoanionic binding of HSO_3^- to the Mo center. This may lead to the formation of a stable intermediate, the ES complex, which would agree well with all the experimental results with native SO and the functional model complex **2**.

With the help of initial investigations, a mechanism can now be established for HSO_3^- oxidation by **1** and **2** catalyzed by SO. The relative energy profile for the overall half-reaction was computed with the fully optimized reaction coordinate in the gas phase and is shown in Figure 4. Each reaction involves an initial transition state (TS1 and TS2), a substrate-bound intermediate (ES1 and ES2), a second transition state (TS3 and TS4), a product-bound second intermediate (EP1 and EP2), and the products (**3** and **4**). The reaction energies are −21.9 ($\Delta G = -28.3$) and −31.1 kcal mol^{-1} ($\Delta G = -18.3$ kcal mol^{-1}) for **1** and **2**, respectively, thus showing that the overall reaction does proceed "downhill" in both the cases. The optimized values of important bond lengths and distances for these states are provided in Table 3, and the optimized geometries are shown in Figure 5.

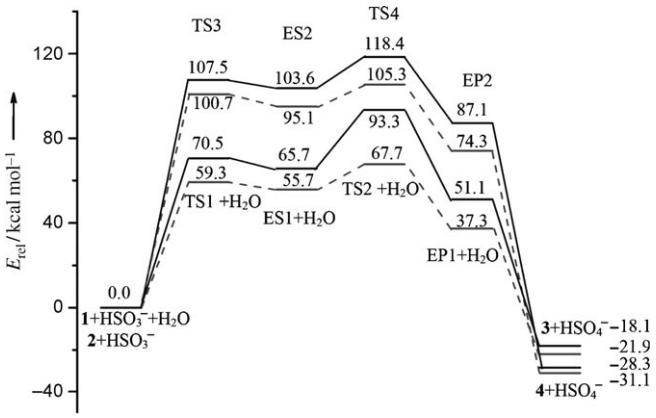

Figure 4. Calculated reaction pathways in the gas phase for the reaction of **1** and **2** with HSO_3^-. – – – = ΔH_{298}, —— = ΔG_{298}.

The first step of the OAT reaction between **1** and HSO_3^- thus proceeds through an initial transition state TS1. This is followed by the formation of a stable intermediate ES1. TS1 is 59.7 kcal mol^{-1} ($\Delta G = 70.5$ kcal mol^{-1}) higher in energy than the rest state and has an Mo–$O_{sulfite}$ distance of 3.031 Å. ES1 is the stable intermediate ($\Delta H = 55.7$, $\Delta G = 65.7$ kcal mol^{-1}) in which the substrate is weakly bound (Mo–$O_{sulfite}$ = 2.194 Å) to the Mo center. Because of the oxoanionic approach of the sulfite, enhancement of the coordination number of the Mo center is required, which moves the SCH_3 group (the O_{ax}–Mo–S_{Me} angle changed by 40°) from an equatorial to an axial position (*trans* to axial oxo group) and results in a distorted octahedral geometry for ES1. This movement of the SCH_3 group was also observed in the theoretically predicted ES complexes of DMSO reductase, trimethyl *N*-oxide reductase, and nitrate reductase.[24] At this stage, the Mo–O_{ax} and Mo–O_{eq} bond lengths

Table 3. Selected bond lengths and distances (Å) of optimized geometry.

Reaction of HSO_3^- with **1**						
Bond	**1**	TS1	ES1	TS2	EP1	**3**
Mo–O_{ax}	1.728	1.725	1.764	1.727	1.732	1.716
Mo–O_{eq}	1.739	1.738	1.737	1.892	2.291	2.405
Mo–$O_{sulfite}$	–	3.031	2.194	–	–	–
Oeq–$S_{sulfite}$	–	–	3.539	2.035	1.510	–
Mo–S1	2.562	2.617	2.722	2.514	2.407	2.373
Mo–S2	2.452	2.408	2.492	2.475	2.404	2.405
Mo–S_{CH3}	2.453	2.481	2.588	2.449	2.438	2.448
Reaction of HSO_3^- with **2**						
Bond	**2**	TS3	ES2	TS4	EP2	**4**
Mo–O_{ax}	1.737	1.737	1.743	1.743	1.706	1.706
Mo–O_{eq}	1.737	1.732	1.724	1.895	2.366	–
Mo–$O_{sulfite}$	–	2.606	2.429	–	–	–
O_{eq}–$S_{sulfite}$	–	–	3.206	2.013	1.502	–
Mo–S1	2.502	2.575	2.608	2.482	2.443	2.455
Mo–S2[a]	2.736	2.771	2.770	2.629	2.469	2.455
Mo–S3	2.502	2.527	2.550	2.571	2.553	2.455
Mo–S4[a]	2.736	2.938	2.932	2.769	2.790	2.455

[a] S atom *trans* to the oxo group.

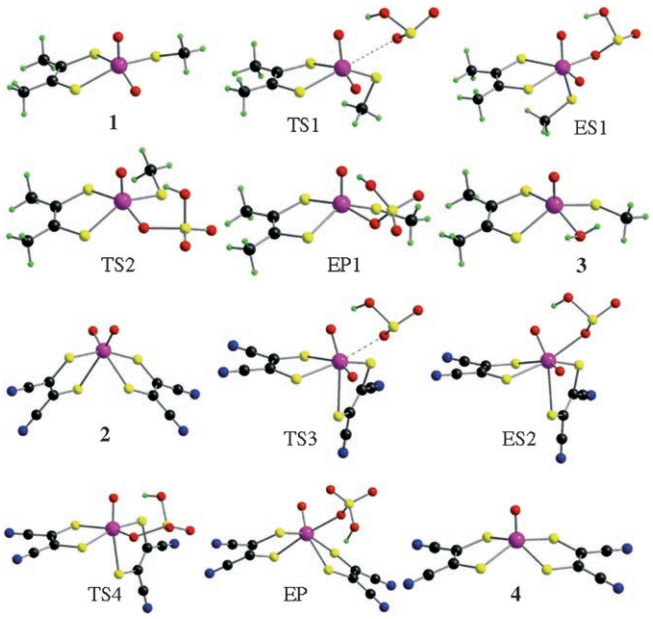

Figure 5. B3LYP gas-phase optimized geometries for **1**, **2**, **3**, **4**, ES1, ES2, EP1, EP2, TS1, TS2, TS3, and TS4.

remain unchanged, and HSO_3^- is oriented such that the S atom of HSO_3^- is directed towards the equatorial oxo group 3.5 Å away. This special orientation of the substrate is influenced by participation of H-bonding of HSO_3^- with the axial oxo group. This controls the disposition of the equatorial oxo group in favor of bonding with the sulfur atom of the substrate in the subsequent reaction step. Energy minima with other orientations of the substrate were not observed. In the search for the ES complex with lone-pair-electron attack, several (on the PES scan point, Figure 3c) full-optimization attempts failed to result in any minima before OAT, in which S (HSO_3^-, substrate) is weakly bound to the O_{eq} group.

The second step of the OAT reaction of **1** passes through a transition state TS2 ($\Delta H = 67.7$, $\Delta G = 93.3$ kcal mol^{-1}) with Mo–O_{eq} and O_{eq}–S(HSO_3^-) distances of 1.892 and 2.035 Å, respectively. TS2 is a six-membered (O_{ax}–Mo–O_{eq}–S–O–H) transition state stabilized by H-bonding similar to that in ES1. The SCH_3 group is again moved to the equatorial position. The energy barrier for this step ($\Delta H = 12$, $\Delta G = 27.6$ kcal mol^{-1}) is much less than for the previous step. The imaginary frequency of 333 cm^{-1} confirmed the saddle-point character between the two stationary states, which corresponds to the stretching vibration modes of Mo–O_{eq} and O_{eq}–S(HSO_3^-). TS2 follows the breaking of the Mo–O_{eq} bond, and product formation takes place via a stable, HSO_4^--bound intermediate EP1 ($\Delta H = 37.3$, $\Delta G = 51.1$ kcal mol^{-1}) with Mo–O_{eq} and O_{eq}–S(HSO_3^-) bond lengths of 2.291 and 1.510 Å, respectively. EP1 is 18.4 kcal mol^{-1} more stable than ES1. At this stage, the OAT reaction is over, and only the oxidized substrate (HSO_4^-) is loosely bound to the product at the Mo^{IV} center. Finally, the reaction concludes with the formation of the water-bound reduced state, $[Mo^{IV}O(S_2C_2Me_2)(H_2O)(SMe)]^{-1}$ (**3**). Model **3** is more stable than the HSO_4^--bound product by 59 kcal mol^{-1} ($\Delta G = 79$ kcal mol^{-1}). The geometrical parameters of **3** are very similar to the structural parameters obtained from the crystal structure of native SO.

The OAT reaction for **2** with HSO_3^- is very similar to that for **1**. The first step of the reaction proceeds through an initial transition state TS3 followed by the formation of a stable intermediate ES2. TS3 is 100.7 kcal mol^{-1} ($\Delta G = 107.5$ kcal mol^{-1}) higher in energy than the rest state and has an Mo–$O_{sulfite}$ distance of 2.606 Å. ES2 is the hexacoordinated intermediate ($\Delta H = 95.1$, $\Delta G = 103.6$ kcal mol^{-1}) in which the Mo–$O_{sulfite}$ bond length is 2.429 Å and one Mo–S(dithioline) bond is elongated to 2.938 Å. At this stage, the Mo–O_{ax} and Mo–O_{eq} bond lengths remain unchanged, and the orientation of HSO_3^- is in a similar H-bonding fashion to that observed in **1**, in which the S atom of HSO_3^- is directed towards the equatorial oxo group at a distance of 3.2 Å.

The second step of the OAT reaction for **2** passes through a transition state TS4 ($\Delta H = 105.3$, $\Delta G = 118.4$ kcal mol^{-1}) with Mo–O_{eq} and O_{eq}–S(HSO_3^-) distances of 1.895 and 2.013 Å, respectively. The nature of TS3 is similar to that of TS2, and the six-membered (O_{ax}–Mo–O_{eq}–S–O–H) transition state is stabilized by H-bonding similar to that in TS2. The energy barrier for this step ($\Delta H = 10.2$, $\Delta G = 15$ kcal mol^{-1}) is very much less than for the previous step. The imaginary frequency of 414 cm^{-1} corresponds to the stretching vibration mode of Mo–O_{eq} and O_{eq}–S(HSO_3^-). TS4 follows the breaking of the Mo–O_{eq} bond, and product formation takes place via a stable, HSO_4^--bound intermediate EP2 ($\Delta H = 74.3$, $\Delta G = 87.1$ kcal mol^{-1}) with Mo–O_{eq} and O_{eq}–S(HSO_3^-) bond lengths of 2.306 and 1.502 Å, respectively. EP2 is 21 kcal mol^{-1} ($\Delta G = 16$ kcal mol^{-1}) more stable than ES2. Finally, the release of the oxidized substrate occurs to form the reduced state of the enzyme, [Mo^{IV}O-

$(mnt)_2]^{2-}$ (**4**). This product-release step is 104 kcal mol^{-1} ($\Delta G = 115$ kcal mol^{-1}) more stable than the HSO_4^--bound product. The geometrical parameters of **4** are very similar to the structural parameters obtained from the crystal structure[10].

The protein environment plays a significant role in the overall reaction pathway. However, the modeling of the native enzyme active site with medium effect needs a great deal of computational resources. We have evaluated only the dielectric effect of the medium on the PES for the overall half-reaction by additional single-point calculations with the solvent effect. The corrected solvation-energy profile obtained with the conductor-like screening model[26] (COSMO) on the gas-phase optimized structure for the reaction of **1** and **2** with HSO_3^- is shown in Figure 6. The solvation energy is seen to stabilize all the transition states and intermediates more than the reactants and products. The overall exothermicity of the OAT reaction and the energy barriers from TS1 to EP1 and TS3 to EP2 do not change significantly. This may be due to the associative nature of the reactant and product molecules in the course of the reaction. In our system, both the reactant and product molecules are negatively charged ions, and their energies were calculated separately. The reactions involve the association of two negatively charged reactants (**1** or **2** and HSO_3^-). Although such a reaction proceeds through the interaction of localized partial charges, the association of two negatively charged ions increases the overall energy of the reaction pathway in the gas phase due to the presence of additional intramolecular repulsive interactions (TS1 to EP1 and TS3 to EP2). Interestingly, the energy differences between the TS and EP states, excluding reactants and products, are nearly the same in the gas phase and in solution (continuum model), whereas the energies of these intermediates and TSs with respect to the reactants in solvent differ from those in the gas phase. This is due to the repulsive interaction between two similarly charged species stabilized in the continuum model. Such stabilization is not observed in the dipole model because of the inherent consideration of the solute surface of the solvent model.[27] An accurate ab initio calculation of solvent effects requires the use of a molecular shape more realistic than a sphere. In the native enzyme, the protein environment may play the important role of minimizing the overall potential-energy barrier by using several noncovalent interactions. The relative energies of the reactant intermediates, TSs, and products for the reaction of **1** and **2** with HSO_3^- in different solvent models with the same basis set, method, and dielectric constant of the medium are shown in Table 4.

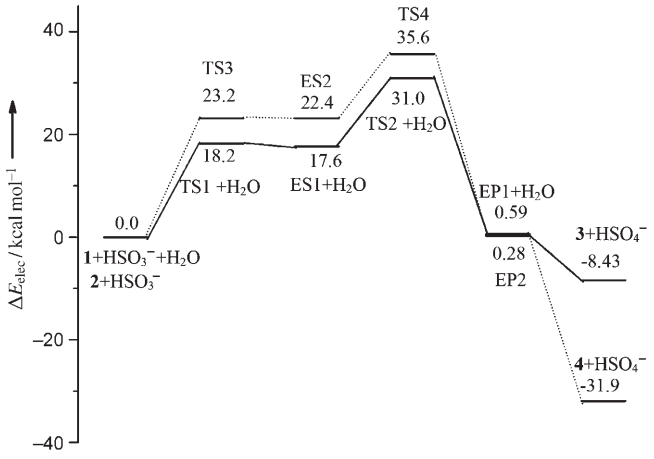

Figure 6. Solvent-corrected energy profile for the reaction of **1** (——) and **2** (·····) with HSO_3^- at 298 K obtained by the COSMO method.

Table 4. Relative single-point energies (kcal mol^{-1}) of reactants, intermediates, TSs, and products for the reaction of **1** and **2** with HSO_3^- in different solvent models and in the gas phase with gas-phase optimized geometry.

	Solvent Model			Gas phase
	COSMO	PCM[a]	Dipole	
Reaction of **1** with HSO_3^-:				
1 + H_2O + HSO_3^-	0.00	0.00	0.00	0.00
TS1 + H_2O	18.21	19.73	50.08	58.78
ES1 + H_2O	17.66	18.82	48.52	54.75
TS2 + H_2O	30.91	31.81	65.51	67.74
EP1 + H_2O	0.59	1.30	33.87	34.95
3 + HSO_4^-	−8.43	−8.95	−15.81	−5.37
Reaction of **2** with HSO_3^-:				
2 + HSO_3^-	0.00	0.00	0.00	0.00
TS3	23.23	24.40	94.33	94.81
ES2	22.40	23.31	93.26	93.74
TS4	35.64	36.64	105.53	104.74
EP2	0.28	0.82	72.64	71.68
4 + HSO_4^-	−31.94	−32.16	−32.26	−31.91

[a] PCM = polarizable continuum model.

Conclusions

In summary, DFT calculations on the synthetic and computational model complexes of SO showed that the OAT reactions involve the formation of the stable intermediate $(MoO_2HSO_3)^-$ through oxoanionic binding of HSO_3^- at the Mo center. The optimized geometries of the ES complexes of **1** and **2** showed a common feature with the participation of hydrogen bonding of the substrate with the axial (spectator) oxo group. This intermediate complex participates in product formation through a six-membered MoO_2HOS transition state, which involves breaking of the Mo–O_{eq} bond with formation of the $S_{sulfite}$–O_{eq} bond. Our results regarding the formation of the Michaelis complex is in agreement with kinetic studies[17a,b,e] on the reductive half-reaction of **2**. This was found to be similar in catalytic behavior to **1** with respect to the reaction with native SO.

Experimental Section

All calculations were performed with the Gaussian 03 (Revision B.04) package.[28] Molecular orbitals were visualized with Gauss View, and geometry-optimized molecular structures were shown with Diamond 3.1e. Geometry optimization, population analysis of molecular orbitals and partial-charge distribution (MPA and NBO method), and relaxed PES scans were carried out at the DFT level. The method used was the Becke three-parameter hybrid-exchange functional,[29a] the nonlocal correlation provided by the Lee, Yang, and Parr expression,[29b] and the Vosko, Wilk, and Nuair 1980 local correlation functional (III) (B3LYP).[29] The 6-31g*+ basis set[30] was used for C, N, and H atoms, and the 6-311g*+ basis set[31] for O and S atoms. The LANL2DZ[32] basis set and LANL2 pseudopotentials of Hay and Wadt[33] were used for the Mo atom. Transition states were optimized with the synchronous transit-guided quasi-Newton (STQN) method.[34] The optimized minima and transition-state structures were characterized by harmonic-vibration-frequency calculations with the same method and basis set in which the minimum has no imaginary frequency and the transition state has only one. Additional single-point energy calculations were carried out on the gas-phase-optimized geometry for medium-effect correction with the same method, basis set, and COSMO with a dielectric constant[35] of 5, radius of 1.4 Å, and temperature of 298 K. The validity of single point energy calculations were also checked with different solvent model. The initial geometry of Mo-co was derived from the reported crystal structure[10] of the native enzyme SO with the considerations that Mo is in the +4 oxidation state and the bond lengths with O_{eq} and O_{ax} are the same (1.71 Å). The initial geometry of **1** was modeled according to native Mo-co. The initial geometry of **2** was obtained from the reported crystal structure.[17a] All geometries were optimized with several possible conformations, and energy minima were considered for further calculations. The initial geometry of **4** was taken from the crystal structure.[36,17d]

Acknowledgements

We thank the CSIR, New Delhi for providing a doctoral fellowship to K.P. and the Department of Science and Technology, New Delhi, for funding.

[1] a) R. Hille, *Chem. Rev.* **1996**, *96*, 2757; b) A. Thapper, C. Lorber, J. Fryxelius, A. Behrens, E. Nordlander, *J. Inorg. Biochem.* **2000**, *79*, 67.

[2] a) R. Hille, *Trends Biochem. Sci.* **2002**, *27*, 360; b) R. Hille, *Met. Ions Biol. Syst.* **2002**, *39*, 187–226.

[3] a) R. Huber, P. Hof, R. O. Duarte, J. J. G. Moura, I. Moura, M.-Y. Liu, J. LeGall, R. Hille, M. Archer, M. J. Romão, *Proc. Natl. Acad. Sci. USA* **1996**, *93*, 8846; b) R. Hille, G. N. George, M. K. Eidsness, S. P. Cramer, *Inorg. Chem.* **1989**, *28*, 4018; c) C. Enroth, B. T. Eger, K. Okamoto, T. Nishino, T. Nishino, E. F. Pai, *Proc. Natl. Acad. Sci. USA* **2000**, *97*, 10723; d) J. J. Truglio, K. Theis, S. Leimkühler, R. Rappa, K. V. Rajagopalan, C. Kisker, *Structure* **2002**, *10*, 115.

[4] a) H.-K. Li, C. Temple, K. V. Rajagopalan, H. Schindelin, *J. Am. Chem. Soc.* **2000**, *122*, 7673; b) G. N. George, J. Hilton, C. Temple, R. C. Prince, K. V. Rajagopalan, *J. Am. Chem. Soc.* **1999**, *121*, 1256; c) J. M. Dias, M. E. Than, A. Humm, R. Huber, G. P. Bourenkov, H. D. Bartunik, S. Bursakov, J. Calvete, J. Caldeira, C. Carneiro, J. J. G. Moura, I. Moura, M. J. Romão, *Structure* **1999**, *7*, 65; d) J. C. Boyington, V. N. Gladyshev, S. V. Khangulov, T. C. Stadtman, P. D. Sun, *Science* **1997**, *275*, 1305; e) M. Jormakka, S. Tornroth, B. Byrne, S. Iwata, *Science* **2002**, *295*, 1863.

[5] K. V. Rajagopalan in *Molybdenum and Molybdenum-Containing Enzymes*, *1st. ed.* (Ed.: M. P. Coughlan), Pergamon Press, Oxford, **1980**.

[6] R. S. Pilato, E. I. Stiefel in *Bioinorganic Catalysis*, *2nd ed.* (Eds.: J. Reedijk, E. Bouwman), Marcel Dekker, New York, **1999**, pp. 81–152.

[7] M. Dixon, E. C. Webb, C. J. R. Throne, K. F. Tipton, *Enzymes*, *3rd ed.*, Academic Press, New York, **1979**.

[8] a) L. G. Howell, I. Fridovich, *J. Biol. Chem.* **1968**, *243*, 5941–5947; b) D. L. Kessler, K. V. Rajagopalan, *J. Biol. Chem.* **1972**, *247*, 6566–6573; c) D. L. Kessler, K. V. Rajagopalan, *Biochim. Biophys. Acta* **1974**, *370*, 399–409.

[9] a) J. L. Johnson, K. V. Rajagopalan, *J. Clin. Invest.* **1978**, *58*, 543–550; b) S. P. Kramer, J. L. Johnson, A. A. Ribeiro, D. S. Mullington, K. V. Rajagopalan, *J. Biol. Chem.* **1987**, *262*, 16357; c) G. N. George, I. J. Pickering, C. Kisker, *Inorg. Chem.* **1999**, *38*, 2539–2540.

[10] C. Kisker, H. Schindelin, A. Pacheco, W. A. Wehbi, R. M. Garrett, K. V. Rajagopalan, J. H. Enemark, D. C. Rees, *Cell* **1997**, *91*, 973–983.

[11] a) H. K. Joshi, J. J. A. Cooney, F. E. Inscore, N. E. Gruhn, D. L. Lichtenberger, J. H. Enemark, *Proc. Natl. Acad. Sci. USA* **2003**, *100*, 3719–3724; b) Y. Izumi, T. Glaser, K. Rose, J. McMaster, P. Basu, J. H. Enemark, B. Hedman, K. O. Hodgson, E. I. Solomon, *J. Am. Chem. Soc.* **1999**, *121*, 10035.

[12] a) C. D. Garner, J. M. Charnock in *Comprehensive Coordination Chemistry*, *Vol. 3* (Eds.: G. Wilkinson, R. D. Gillard, J. A. McCleverty), Pergamon Press, New York, **1987**, pp. 1329–1374; b) E. I. Stiefel in *Comprehensive Coordination Chemistry*, *Vol. 3* (Eds.: G. Wilkinson, R. D. Gillard, J. A. McCleverty), Pergamon Press, New York, **1987**, pp. 1375–1420; c) C. D. Garner in *Comprehensive Coordination Chemistry*, *Vol. 3* (Eds.: G. Wilkinson, R. D. Gillard, J. A. McCleverty), Pergamon Press, New York, **1987**, pp. 1421–1444; d) Z. Dori in *Comprehensive Coordination Chemistry*, *Vol. 3* (Eds.: G. Wilkinson, R. D. Gillard, J. A. McCleverty), Pergamon Press, New York, **1987**, pp. 973–1022; e) J. H. Enemark, J. J. A. Cooney, J.-J. Wang, R. H. Holm, *Chem. Rev.* **2004**, *104*, 1175–1200; f) S. F. Gheller, B. E. Schultz, M. J. Scott, R. H. Holm, *J. Am. Chem. Soc.* **1992**, *114*, 6934.

[13] a) R. H. Holm, *Coord. Chem. Rev.* **1990**, *100*, 183–221; b) R. H. Holm, *Chem. Rev.* **1987**, *87*, 1401–1449; c) B. E. Schultz, S. F. Gheller, M. C. Muetterties, M. J. Scott, R. H. Holm, *J. Am. Chem. Soc.* **1993**, *115*, 2714; d) Z. Xiao, C. G. Young, J. H. Enemark, A. G. Wedd, *J. Am. Chem. Soc.* **1992**, *114*, 9194; e) Z. Xiao, M. A. Bruck, J. H. Enemark, C. G. Young, A. G. Wedd, *Inorg. Chem.* **1996**, *35*, 7508; f) S. A. Roberts, C. G. Young, W. E. Cleland, R. B. Ortega, J. H. Enemark, *Inorg. Chem.* **1988**, *27*, 3044; g) J. M. Berg, R. H. Holm, *J. Am. Chem. Soc.* **1985**, *107*, 917; h) C. J. Doonan, D. A. Slizys, C. G. Young, *J. Am. Chem. Soc.* **1999**, *121*, 6430; i) H. Arzoumanian, R. Lopez, G. Agrifoglio, *Inorg. Chem.* **1994**, *33*, 31779.

[14] a) B. E. Schultz, R. H. Holm, *Inorg. Chem.* **1993**, *32*, 4244; b) G. C. Tucci, J. P. Donahue, R. H. Holm, *Inorg. Chem.* **1998**, *37*, 1602–1608; c) C. Lorber, M. R. Plutino, L. I. Elding, E. Nordlander, *J. Chem. Soc. Dalton Trans.* **1997**, 3997–4004.

[15] a) M. A. Pietsch, M. B. Hall, *Inorg. Chem.* **1996**, *35*, 1273–1278; b) L. M. Thomson, M. B. Hall, *J. Am. Chem. Soc.* **2001**, *123*, 3995–400; c) A. K. Rappé, W. A. Goddard III, *J. Am. Chem. Soc.* **1982**, *104*, 3287; d) Y. Izumi, T. Glaser, K. Rose, J. McMaster, P. Basu, J. H. Enemark, B. Hedman, K. O. Hodgson, E. I. Solomon, *J. Am. Chem. Soc.* **1999**, *121*, 10035.

[16] a) V. N. Nemykin, J. Laskin, P. Basu, *J. Am. Chem. Soc.* **2004**, *126*, 8604–8605; b) P. D. Smith, D. Millar, J. Andrew, C. G. Young, A. Ghosh, P. Basu, *J. Am. Chem. Soc.* **2000**, *122*, 9298–9299.

[17] a) S. K. Das, P. K. Chaudhury, D. Biswas, S. Sarkar, *J. Am. Chem. Soc.* **1994**, *116*, 9061–9070; b) P. K. Chaudhury, S. K. Das, S. Sarkar, *Biochem. J.* **1996**, *319*, 953–959; c) P. K. Chaudhury, K. Nagarajan, A. Kumar, R. Maiti, S. K. Das, S. Sarkar, *Indian J. Chem. Sect. A* **2003**, *42*, 2223; d) R. Maiti, K. Nagarajan, S. Sarkar, *J. Mol. Struct.* **2003**, *656*, 169–176; e) P. K. Chaudhury, K. Nagarajan, P. Dubey, S. Sarkar, *J. Inorg. Biochem.* **2004**, *98*, 1667–1677.

[18] S. K. Das, PhD thesis, Indian Institute of Technology, Kanpur (India), **1996**.

[19] a) M. S. Brody, R. Hille, *Biochim. Biophys. Acta* **1995**, *133*, 1253; b) R. Hille, *J. Biol. Inorg. Chem.* 1997, ***2***, 804.
[20] A. Thapper, R. J. Deeth, E. Nordlander, *Inorg. Chem.* **1999**, *38*, 1015–1018.
[21] K. Peariso, R. L. McNaughton, M. Kirk, *J. Am. Chem. Soc.* **2002**, *124*, 9006–9007.
[22] K. Nagarajan, P. K. Chaudhury, B. R. Srinivasan, S. Sarkar, *Chem. Commun.* **2001**, 1786–1787.
[23] The low-pH milieu in mitochondria suggests the presence of HSO_3^- as the major species along with SO_3^{2-}. Hence, HSO_3^- is used as the substrate for SO, Mo-co, **1**, and **2.**
[24] a) C. E. Webster, M. B. Hall, *J. Am. Chem. Soc.* **2001**, *123*, 5820; b) A. Thapper, R. J. Deeth, E. Nordlander, *Inorg. Chem.* **2002**, *41*, 6695; c) M. Leopoldini, M. Toscano, M. Dulak, T. A. Wesolowski, *Chem. Eur. J.* **2006**, *12*, 2532–2541.
[25] B. S. Lim, M. W. Willer, Mingming Miao, R. H. Holm, *J. Am. Chem. Soc.* **2001**, *123*, 8343.
[26] a) A. Klamt, G. Schuurmann, *J. Chem. Soc. Perkin Trans. 2.* **1993**, 779–805; b) A. Klamt, V. Jonas, T. Burger, J. C. Lohrenz, *J. Phys. Chem. A* **1998**, *102*, 5074–5085; c) A. Schafer, A. Klamt, D. Sattel, J. C. W. Lohrenz, F. Eckert, *Phys. Chem. Chem. Phys.* **2000**, *2*, 2187–2193.
[27] The dipole model treats the solute as a sphere of symmetrical electric charge produced by a dipole, whereas the continuum model considers the cavity as a union of a series of interlocking atomic spheres of different partial surface charges.
[28] Gaussian 03 (Revision B.05), M. J. Frisch, G. W. Trucks, H. B. Schlegel, G. E. Scuseria, M. A. Robb, J. R. Cheeseman, J. A. Montgomery, Jr., T. Vreven, K. N. Kudin, J. C. Burant, J. M. Millam, S. S. Iyengar, J. Tomasi, V. Barone, B. Mennucci, M. Cossi, G. Scalmani, N. Rega, G. A. Petersson, H. Nakatsuji, M. Hada, M. Ehara, K. Toyota, R. Fukuda, J. Hasegawa, M. Ishida, T. Nakajima, Y. Honda, O. Kitao, H. Nakai, M. Klene, X. Li, J. E. Knox, H. P. Hratchian, J. B. Cross, C. Adamo, J. Jaramillo, R. Gomperts, R. E. Stratmann, O. Yazyev, A. J. Austin, R. Cammi, C. Pomelli, J. W. Ochterski, P. Y. Ayala, K. Morokuma, G. A. Voth, P. Salvador, J. J. Dannenberg, V. G. Zakrzewski, S. Dapprich, A. D. Daniels, M. C. Strain, O. Farkas, D. K. Malick, A. D. Rabuck, K. Raghavachari, J. B. Foresman, J. V. Ortiz, Q. Cui, A. G. Baboul, S. Clifford, J. Cioslowski, B. B. Stefanov, G. Liu, A. Liashenko, P. Piskorz, I. Komaromi, R. L. Martin, D. J. Fox, T. Keith, M. A. Al-Laham, C. Y. Peng, A. Nanayakkara, M. Challacombe, P. M. W. Gill, B. Johnson, W. Chen, M. W. Wong, C. Gonzalez, J. A. Pople, Gaussian, Inc., Pittsburgh, PA (USA), **2003**.
[29] a) A. D. Becke, *J. Chem. Phys.* **1993**, *98*, 5648; b) C. Lee, W. Yang, R. G. Parr, *Phys. Rev. B* **1988**, *37*, 785.
[30] G. A. Patersson, M. A. Al-Laham, *J. Chem. Phys.* **1991**, *94*, 6081.
[31] A. D. McLean, G. S. Chandler, *J. Chem. Phys.* **1980**, *72*, 5639.
[32] P. J. Hay, W. R. Wadt, *J. Chem. Phys.* **1985**, *82*, 299.
[33] a) P. J. Hay, W. R. Wadt, *J. Chem. Phys.* **1985**, *82*, 270–283; b) W. R. Wadt , P. J. Hay, *J. Chem. Phys.* **1985**, *82*, 284–298.
[34] C. Peng, Y. Alaya, B. Schlegel, M. J. Frisch, *J. Comput. Chem.* **1996**, *17*, 49.
[35] Dielectric constants of 3–5 are often employed to mimic the protein environment. We chose a value of 5: a) P. E. Smith, R. M. Brunne, A. E. Mark, W. F. van Gunsteren, *J. Phys. Chem.* **1993**, *97*, 2009–2014; b) G. Löffler, H. Schrelber, O. Stelnhauser, *J. Mol. Biol.* **1997**, *270*, 520–534; c) F. Ogliaro, S. P. de Visser, S. Cohen, P. K. Sharma, S. Shaik, *J. Am. Chem. Soc.* **2002**, *124*, 2806–2814.
[36] H. Oku, N. Ueyama, A. Nakamura, Y. Kai, N. Kanehisa, *Chem. Lett.* **1994**, 607.

Received: January 24, 2007
Revised: April 24, 2007
Published online: June 28, 2007

